

PAPER • OPEN ACCESS

## Thermo-elasto-viscoplastic constitutive laws for metallic alloys during their solidification

To cite this article: G M Laschet and H Behnken 2019 *IOP Conf. Ser.: Mater. Sci. Eng.* **529** 012083

View the [article online](#) for updates and enhancements.



**IOP | ebooks™**

Bringing you innovative digital publishing with leading voices to create your essential collection of books in STEM research.

Start exploring the **collection** - download the first chapter of every title for free.

# Thermo-elasto-viscoplastic constitutive laws for metallic alloys during their solidification

**G M Laschet and H Behnken**

ACCESS e.V., RWTH Aachen University, Intzestrasse 5, D-52072 Aachen, Germany

{g.laschet, h.behnken}@access.rwth-aachen.de

**Abstract.** To describe the thermomechanical behaviour of the semi-solid state during alloy solidification, specific viscoplastic constitutive laws are derived for the coherent and non-coherent regime of the mush. For the coherent semi-solid regime an original viscoplastic flow potential is derived, which includes micro-structural parameters. This potential takes also isotropic hardening, pressure dependence of yielding and the strength difference in tension and compression into account. For the non-coherent mushy state of suspensions under shear loading, a simplified viscoplastic potential is adopted by neglecting pressure effects on the solid dendrites. Continuity at mechanical coherency is imposed and allows the reduction of the model parameters of the non-coherent regime. The developed constitutive laws are implemented in Abaqus via a user-defined CREEP routine. Simulations of uniaxial tension, compression or pure shear experiments allow identifying the model parameters of an A356 aluminium alloy.

## 1. Introduction

During casting, most technical alloys solidify with the formation of a two-phase region known as the mushy zone. They undergo a continuous transition from the liquid to the solid state. The solidification starts below the liquidus temperature by local undercooling and the nucleation of solid germs takes place. At low solid fractions, dendritic germs grow independently and are free to move in the melt. As solidification progresses, interactions between dendrites occur and the mush develops the first shear strength due to dendrites entanglement. For higher solid fractions, dendrites interlock, solid skeletons are built and the mush reaches mechanical coherence. At that state, the solid skeleton densifies under external pressure or dilates under tensile loading. Toward the end of solidification, solid grains start to coalesce and liquid feeding drops drastically. The complexity of the solid-liquid interactions at the micro-scale makes their characterization and rheological modelling difficult and delicate.

Deformations in the coherent mushy zone are influenced by the viscoplastic solid skeleton and the flow of remaining viscous melt in the pore space. In the literature some models were proposed to describe the coherent mushy zone behaviour. Martin et al [1, 2] developed a two-phase isothermal model, which is able to characterize the compressibility and hardening/softening behaviour of the fluid saturated solid and to address the hydrostatic pressure dependence of the yield surface. Ludwig et al. [3] generalized Martin's rheological models by deriving it from a viscoplastic potential and by introducing the coalescence solid fraction  $g_{\text{coal}}$  in its formulation. To address hot tears initiation, Mihanyar et al [4] extended Ludwig's model by introducing an additional internal variable measuring the de-cohesion of the solid skeleton under tensile deformations. All these rheological models of the coherent mushy zone [1-4] were derived from models describing the hot deformation of porous materials [5]. These models have been validated for porosities up to 10%, which corresponds to high solid fractions



( $0.9 \leq g_s \leq 1$ ), where hot tears can appear at the end of the solidification. For lower solid fractions between traction coherency ( $g_{C,tr} \approx 0.51$  for AlSi<sub>7</sub>Mg alloy) and  $g_s \approx 0.80$ , their validity has not yet been shown. These models are also not linked to a viscoplastic constitutive law for the non-coherent mushy regime.

Therefore, the aim of this paper is to develop for each semi-solid regime (coherent and non-coherent) a specific constitutive law depending on microstructural features like fraction solid and grain size, which are extracted from a coupled multi-phase field simulation of the microstructure evolution [6]. Effects observed experimentally for Al-Cu alloys [2,3] and AlSi<sub>7</sub>Mg [7], like isotropic hardening, pressure dependence of yielding and the strength difference effect in tension and compression, have to be addressed in the formulation of the constitutive law for the coherent mushy regime. However, the observed softening behaviour under tensile loading is not yet addressed here.

Based on the theory of porous media, the specific thermo-elasto-viscoplastic constitutive laws for both mushy regimes are derived in section 2 and linked together at traction coherency. In section 3, the parameters of both constitutive laws are identified for an A356 aluminium alloy via FE simulations of uniaxial tension, compression and pure shear tests.

## 2. Thermomechanical constitutive laws

In casting and welding processes, the temperature varies strongly from above the melting point to room temperature. Therefore, the material response must reproduce either elastoplastic behaviour at room temperature or pure viscous behaviour of the melt above the liquidus temperature  $T_{liq}$ . The transition can be simulated by developing appropriate thermo-elasto-viscoplastic constitutive laws for each material state (liquid, mushy and solid) along the cooling path. Moreover, each constitutive law for a specific regime has to vary *continuously* to the next one at specific temperatures like  $T_{sol}$  (solidus temperature),  $T_{liq}$  or at specific solid fractions like  $g_{C,sh}$  (shear coherency) and  $g_{C,tr}$  (traction coherency).

Since the deformation in casting and welding is mainly driven by thermal deformation we adopt here the geometrical linear approach and use the porous media formalism, detailed elsewhere [8]. In this framework, the constitutive law is formulated on the solid skeleton and written using the effective solid stress tensor  $\boldsymbol{\sigma}_E^s$ , which takes the effect of the liquid pressure  $p_l$  on the solid phase into account via expression:  $\boldsymbol{\sigma}_E^s = \boldsymbol{\sigma} + p_l \mathbf{I}$ , where  $\boldsymbol{\sigma}$  is the total (applied) stress in a point and  $\mathbf{I}$  is the second order identity tensor. The total strain tensor is computed in terms of the displacement field of the solid phase  $\mathbf{u}^s$  by:  $\boldsymbol{\epsilon}(\mathbf{u}^s) = \frac{1}{2}(\nabla \mathbf{u}^s + \nabla^T \mathbf{u}^s)$  and its volumetric and deviatoric parts are given respectively by:

$$e^{vol} = \text{tr}(\boldsymbol{\epsilon}) = \nabla \cdot \mathbf{u}^s \quad ; \quad \mathbf{E} = \text{dev}(\boldsymbol{\epsilon}) = \boldsymbol{\epsilon} - \frac{1}{3}e^{vol}\mathbf{I}. \quad (1)$$

Moreover, the total volumetric strain  $e^{vol}$  can be additively decomposed into elastic, viscoplastic and thermal contributions; whereas the total deviatoric strain  $\mathbf{E}$  is split only in an elastic  $\mathbf{E}^e$  and viscoplastic part  $\mathbf{E}^{vp}$ . Similarly, the effective stress tensor  $\boldsymbol{\sigma}_E^s$  on the solid can be split into its hydrostatic and deviatoric parts  $p_s$  and  $\mathbf{S}_s$ , where  $p_s$  is the effective pressure on the skeleton (taken positive in compression):  $p_s = -\frac{1}{3}\text{tr}(\boldsymbol{\sigma}_E^s)$  and  $\mathbf{S}_s = \boldsymbol{\sigma}_E^s - \frac{1}{3}\text{tr}(\boldsymbol{\sigma}_E^s)\mathbf{I}$ .

As suggested in ref. [9], the effective stress of the solid phase is governed by following split of the isotropic Hooke law:

$$p_s = \frac{B(T, \mathbf{V}_k)}{g_s} (e^{vol} - e^{th}), \quad (2)$$

$$\mathbf{S}_s = \frac{2G(T, \mathbf{V}_k)}{g_s} \mathbf{E}^e = \frac{2G(T, \mathbf{V}_k)}{g_s} (\mathbf{E} - \mathbf{E}^{vp}), \quad (3)$$

where  $G(T, \mathbf{V}_k)$  is the shear modulus,  $B(T, \mathbf{V}_k)$  the bulk modulus and  $e^{th}$  denote the volumetric thermal strain, which is composed of the thermal expansion and shrinkage terms. The shrinkage term expresses the liquid to solid phase transformation. Both modules depend on the temperature  $T$  and on the internal variable vector  $\mathbf{V}_k = \{V_1, V_2, \dots, V_k\}$ , which involves fraction solid  $g_s$  and additional microstructural features like grain size, dendrite arm spacing, and so on. Their effective values for a given fraction solid are determined by homogenization runs for equiaxed and directional microstructures respectively. These

microstructures have been predicted by the multi-phase field model directly linked to the thermomechanical casting simulation, as outlined in ref. [6].

N.B.: During the liquid to solid phase change, the solid fraction starts from  $g_s = 0$ , while the stresses remain bounded. As a consequence, both the volumetric and deviatoric elastic strains vanish at  $T_{liq}$  and Eq. (2) reduces to  $e^{vol} = e^{th}$ ; whereas Eq. (3) becomes  $\mathbf{E} = \mathbf{E}^{vp}$  so that only pure viscoplastic shear deformations occur above  $T_{liq}$ .

### 2.1 Constitutive model for the coherent mushy zone

a) To simulate deformations during solidification, the underlying viscoplastic model has to address the compressibility of the mush at the macro-scale due to the change of pore structure as well as the strain rate and hydrostatic pressure dependency. Moreover, it has to describe continuously the coherent mushy behaviour from traction coherency up to the solid state. In general, for porous materials, their viscoplastic potential  $\Omega^{vp}$  can be written in terms of the effective stress tensor  $\sigma_E^s$ . Relying on ideas developed in [8, 10], we define the following viscoplastic potential for the coherent mush:

$$\Omega^{vp}(e^{vp}, T, \mathbf{V}_k) = \frac{1}{(n+1)[C(\text{Tr}, \mathbf{V}_k).K]^n} \langle \sigma_{vM}^2 - a_0^2(e^{vp}, \mathbf{V}_k) + a_2(\text{Tr}, \mathbf{V}_k) p_s^2 \rangle^{\frac{n+1}{2}}, \quad (4)$$

where  $\sigma_{vM}$  is the equivalent von Mises stress of the effective stress tensor  $\sigma_E^s$ ;  $e^{vp}$  is the equivalent viscoplastic strain;  $K$  the viscoplastic consistency of the mush;  $n$  the strain rate sensitivity parameter;  $\text{Tr} = \frac{p_s}{\sigma_{vM}}$  specifies the stress triaxiality factor and  $C$  an internal variable describing the state of cohesion of the mush introduced firstly by Martin et al [2]. The scalar term  $a_0$  of the generalized yield function (in Macaulay brackets) defines the isotropic strain hardening behaviour by:

$$a_0(e^{vp}, T, \mathbf{V}_k) = Y_0 + [q(1 - \exp(-b e^{vp})) + h e^{vp}].g_s, \quad (5)$$

where  $Y_0$  is the initial yield stress;  $b$  and  $q$  are the Voce exponent and coefficient respectively and  $h$  specifies a linear hardening coefficient.

N.B: All material parameters of the alloy depend on the temperature, fraction solid  $g_s$  and on relevant microstructural features  $\mathbf{V}_k$ . To facilitate the paper reading, these dependencies will be not mentioned explicitly in each expression hereafter.

b) The hydrostatic pressure coefficient  $a_2$  is defined as a function of  $g_s$  by following expression:

$$a_2(\text{Tr}) = AA(\text{Tr}). \frac{(g_s - g_{c, \text{tr}})}{(1 - g_{c, \text{tr}})} \cdot (1 - g_s)^d. \quad (6)$$

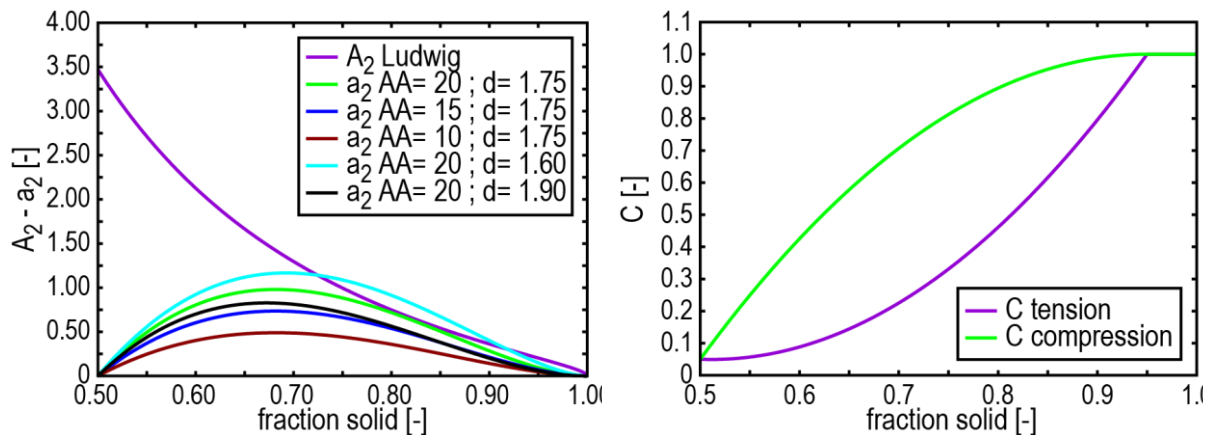


**Figure 1:** Variation of the hydrostatic coefficient  $a_2$  with the fraction solid  $g_s$  for different combinations of coefficient  $AA$  and exponent  $d$  and for Ludwig's coefficient  $A_2$  (left). Variation of internal cohesion variable  $C$  with the fraction solid (right).

Expression (6) guarantees the continuity of  $a_2$  to both extremal cases: the solid state on one side and the non-coherent regime on the other side. Indeed,  $a_2(g_s = 1) = 0$  and  $a_2(g_s = g_{C,tr}) = 0$ . This expression differs from Ludwig's pressure coefficient  $A_2$  [3]:  $A_2 = \frac{9}{4} \left[ n \left( \frac{1}{(1-g_s)^n} - 1 \right) \right]^{\frac{-2n}{n+1}}$ . Indeed, as shown in Figure 1.left for the Al-Cu4% alloy with  $n = 3.8$ , Ludwig's  $A_2$  coefficient leads to unrealistic large pressure contributions nearly the traction coherency; whereas expression (6) reduces to zero near  $g_{C,tr}$ . Impact of varying exponent  $d$  and coefficient  $AA$  in their respective definition range on the pressure coefficient  $a_2$  is outlined also on Figure 1.left. The results show that the combination  $AA = 20$ ;  $d = 1.75$  provides a similar pressure term as Ludwig's  $A_2$  at high solid fractions:  $g_s \in [0.75, 1]$ .

c) An internal variable  $C$  has been introduced in the viscoplastic potential (4) in order to take partial cohesion of the solid skeleton into account.  $C = 1$  corresponds to a fully cohesive mush, when coalescence happens at the end of the solidification. Indeed, at coalescence ( $g_{coal} \approx 0.95$ ), liquid is still present in isolated pockets at grain boundaries. Following Ludwig [3], we assume that  $C = 1$  when  $g_s \geq g_{coal}$ . The much weaker response in tension than in compression of the partially solidified alloy is rendered in the present model via a different evolution of  $C$  with  $g_s$  in tension and compression. Contrary to Ludwig's et al. [3] approach, in which  $C$  is expressed by a complex evolution law of the deformation rate  $\mathbf{D}^{vp}$ , we introduce following simple expressions for  $C(g_s, Tr)$  in the solid fraction range  $g_{C,tr} \leq g_s \leq g_{coal}$  (see Figure 1.right):

$$\text{ - if } Tr > 0 : \quad C = 1 - (1 - g_{C,tr}) \cdot \left( \frac{g_{coal} - g_s}{g_{coal} - g_{C,tr}} \right)^2, \quad (7.a)$$

$$\text{ - if } Tr \leq 0 : \quad C = \left( \frac{g_s - g_{C,tr}}{g_{coal} - g_{C,tr}} \right)^2 + C_{coh} \cdot \frac{(g_{coal} - g_s)}{(g_{coal} - g_{C,tr})}, \quad (7.b)$$

where  $C_{coh}$  is an initial cohesion value at traction coherency: we assume  $C_{coh} \approx 0.05$ .

Figure 1.right shows that, above  $g_s = 0.75$ , the cohesion term  $C$  decreases slowly in compression due to interlocking dendrites; whereas in tension, a stronger decrease happens as liquid regions expand at grain boundaries.

d) As classical for J2 viscoplastic behaviour of metals, the inelastic strain rate  $\mathbf{D}^{vp}$  is given here also by an associated flow rule:

$$\mathbf{D}^{vp} = -\frac{1}{3} \frac{\partial \Omega^{vp}}{\partial p_s} \mathbf{I} + \frac{\partial \Omega^{vp}}{\partial \sigma_{VM}} \cdot \left( \frac{3}{2} \frac{\mathbf{S}_s}{\sigma_{VM}} \right) = \frac{1}{(C.K)^n} \langle \sigma_{VM}^2 - a_0^2 + a_2 p_s^2 \rangle^{\frac{n-1}{2}} \cdot \left[ -\frac{a_2}{3} p_s \mathbf{I} + \frac{3}{2} \frac{\mathbf{S}_s}{\sigma_{VM}} \right]. \quad (8)$$

As equation (8) depends linearly from the hydrostatic pressure, it addresses well densification in compression and swelling in tension of the fluid saturated skeleton. Note that the pressure dependence of  $\mathbf{D}^{vp}$  disappears at traction coherency as  $a_2$  vanishes there. Moreover, equation (8) insures that the strain rate  $\mathbf{D}^{vp}$  varies continuously if the local tensile state becomes compressive during solidification or if the inverse situation happens.

## 2.2 Constitutive model for the non-coherent mushy zone

Below the traction coherency, the solidifying dendrites move individually in the mush. However, shear ramp and jump tests in a rheometer on suspensions with  $g_s \in [0.25, 0.35]$  have shown that the mush presents some shear resistance with a low yield stress (in kPa) (see §3.2). To describe the viscoplastic behaviour of suspensions, we consider only shear loading, implying  $Tr = 0$ , assume that the hydrostatic pressure effect disappears ( $a_2 = 0$ ) and introduce following simplified viscoplastic potential:

$$\Omega^{vp}(e^{vp}) = \frac{A}{(n+1)K^n} \langle \sigma_{VM} - a_0(e^{vp}) \rangle^{(n+1)}, \quad (9)$$

where  $A = \frac{\exp[w \cdot f(g_s)]}{U}$  with  $f(g_s) = \frac{g_{C,tr} - g_s}{g_{C,tr} - g_{C,sh}}$  (10)

and  $g_{C,sh}$  specifies the shear coherency fraction solid at which first small shear stresses are measured experimentally: shear jump tests on A356 suspensions reveal  $g_{C,sh} \approx 0.22$  [11].

At traction coherency,  $f(g_{C,tr}) = 0$  and  $A$  reduces to  $\frac{1}{U}$ . By multiplying the Macaulay brackets, it becomes:  $\frac{1}{(n+1)U.K^n}$ . On the other side, the same term of the viscoplastic potential (4) for the coherent mushy zone writes at  $g_{C,tr}$ :  $\frac{1}{(n+1)[C_{coh}K]^n}$ . The *continuity* at traction coherency of both viscoplastic constitutive laws implies that both factors are identical, which implies:  $U = C_{coh}^n$ . Thus, only *one additional material parameter*  $w$  is introduced to specify the viscoplastic potential (9) and the associated viscoplastic flow rule becomes:

$$\mathbf{D}^{vp} = \frac{\exp[w(V_k).f(g_s)]}{(C_{coh}.K)^n} \langle \sigma_{vM} - a_0 \rangle^n \cdot \left[ \frac{3}{2} \frac{S_s}{\sigma_{vM}} \right]. \quad (11)$$

### 2.3 Liquid-like constitutive law

At shear coherency  $g_{C,sh}$ , we have  $f(g_s) = 0$  and assume that the hardening coefficients  $q$ ,  $h$  become zero and disappear from coefficient  $a_0$  (see Eq. (5)), so that  $a_0$  equals the low initial yield stress  $Y_{0,sh}$ . Below this fraction solid,  $Y_0$  reduces strongly with temperature increase and vanishes near  $T_{liq}$ , so that the viscoplastic flow rule (11) reduces to:

$$\mathbf{D}^{vp} = \frac{3}{2(C_{coh}.K)^n} \sigma_{vM}^{n-1} \cdot \mathbf{S} = \eta^m \sigma_{vM}^{n-1} \cdot \mathbf{S} \quad (12)$$

where  $\eta$  is the viscosity of the suspensions and  $m = 1/n$ .

As the rate sensitivity coefficient  $n$  differs usually from one in presence of growing dendritic germs, law (12) expresses a non-Newtonian Norton-Hoff viscoplastic flow. Above  $T_{liq}$ , coefficient  $n$  is set to one, so that the melt becomes a Newtonian fluid and law (12) reduces to a pure *viscous law* given by:

$$\mathbf{S} = \eta \cdot \mathbf{D}^{vp} \quad (13)$$

### 2.4 Constitutive law for the solid phase

Below the solidus temperature  $T_{sol}(g_s = 1)$ , the hydrostatic pressure dependence disappears ( $a_2 = 0$ ) and the viscoplastic potential (Eq. 4) reduces to a classical Lemaitre & Chaboche potential [12]:

$$\Omega^{vp}(e^{vp}, T) = \frac{1}{(n+1)K^n} \langle \sigma_{vM} - a_0(T, e^{vp}) \rangle^{(n+1)} \quad (14)$$

This potential describes a coupled isotropic *strain hardening* – *viscosity* material behaviour, whose associated flow rule is given by:

$$\mathbf{D}^{vp} = \left\langle \frac{\sigma_{vM} - a_0}{K} \right\rangle^n \cdot \left[ \frac{3}{2} \frac{S_s}{\sigma_{vM}} \right] \quad (15)$$

## 3. Model parameter identification for uniaxial tests on A356 alloy

The constitutive laws for each semi-solid regime have been implemented as user defined CREEP routine in the FE program Abaqus. For each experimental flow curve ( $\sigma_{vM}$ ,  $e^{vp}$ ) at a given temperature (see ref. [7], [11]), the uniaxial strain rate  $D^{vp}$  and the fraction solid  $g_s$  are known. Note that  $g_s$  differs strongly in remelting and solidification tests, indicating a pronounced hysteresis behaviour. In the coherent mushy regime, the rate sensitivity exponent  $n$  is quasi constant for Al alloys:  $n = 3.8$  (see ref. [3]). Under quasi-static conditions and by neglecting the hydrostatic pressure term, we get following expression:

$$\sigma_{vM} = D^{vp}(C.K)^n + Y_0 + [q(1 - \exp(-be^{vp})) + h e^{vp}].g_s, \quad (16)$$

where the first two terms correspond to the experimental yield stress  $Y_{\text{exp}}$ . Knowing internal cohesion  $C(g_s)$  via expressions (7) and taking a 1<sup>st</sup> guess for  $K(T)$  from measurements [13], we calculate the yield stress  $Y_0$ .

At next, a least-square fit is performed in order to identify the unknown isotropic hardening parameters:  $q$ ,  $b$  and  $h$ . Then, the uniaxial tension, compression and shear experiments are simulated in Abaqus by using mixed hybrid elements with the implemented constitutive laws. This way, the 1<sup>st</sup> guess of viscoplastic consistency  $K$  will be improved and the parameters  $AA$  (coherent mush model),  $w$  and  $n$  (non-coherent mush model) will be identified.

### 3.1 Remelting tests in compression and tension

Round as cast A356 bars ( $\phi = 20$  mm) are heated up at a rate of  $0.5$  °C s<sup>-1</sup> to testing temperature. After a holding time of 120 s, constant tensile or compressive strain rates of  $0.005$  s<sup>-1</sup> are applied. In Figure 2 are drawn the measured flow curves in uniaxial tension and compression tests at  $565$ °C and  $570$ °C respectively. These curves illustrate the strong different behaviour in tension and compression of remelted specimens. In table 1, the fitted quasi-static material parameters for each uniaxial test are outlined. In tension, the yield stress is larger than in compression, but the maximum tensile stress occurs at low strains. Moreover, strong softening is observed due to decohesion at grain boundaries. In compression, the initial yield stresses are small, but significant strain hardening happens, which is characterized by larger Voce coefficients  $q$ , mainly at higher solid fractions. Additionally, the creep FE simulations permit to quantify the impact of the pressure term  $a_2$  (Eq. (6)) by varying coefficient  $AA$  within  $AA \in [10, 20]$  and taking exponent  $d$  fixed ( $d = 1.75$ ). At  $570$ °C and  $g_s = 0.791$ , the impact of coefficient  $AA$  is significant (see Figure 2): coefficient  $AA = 10$  induces too large hardening increase mainly in compression; whereas  $AA=15$  and  $AA=20$  lead to accurate flow curve predictions in tension and compression. Impact of coefficient  $AA$  is strongly reduced at higher fractions solid, as flow curve predictions at  $565$ °C illustrate on Figure 2.right. Moreover, these creep FE simulations allow us, at each temperature, to derive a tuned viscoplastic consistency  $K$ , outlined in table 1.

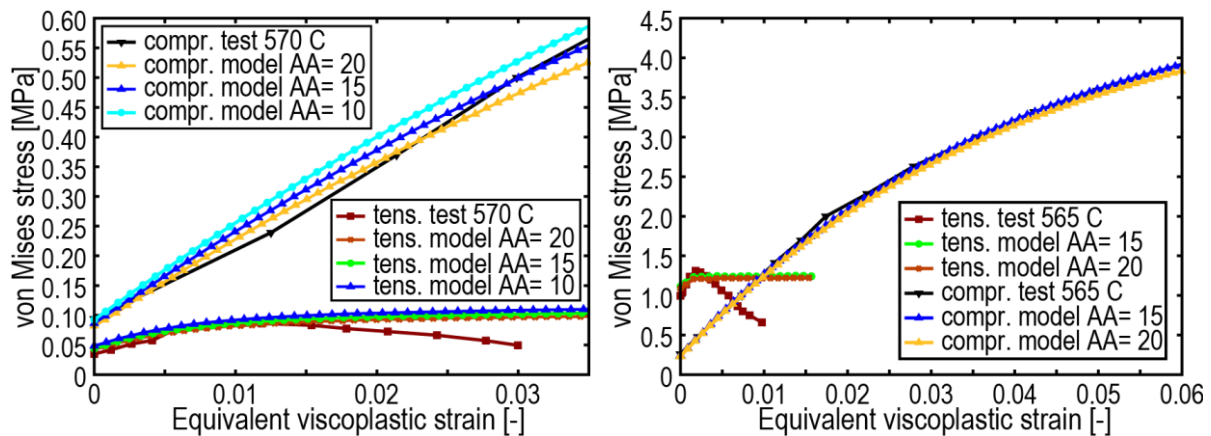


**Figure 2:** Identification of uniaxial compression and tension tests at strain rate  $D^{\text{vp}} = 0.005$  s<sup>-1</sup> on remelted A356 semi-solid alloys at  $570$ °C (left) and  $565$ °C (right) respectively.

**Table 1:** Fitted material parameters of the coherent mush model for compression and tension tests. Superscripts  $C$  and  $T$  indicate the compression and tensile test respectively.

T [°C]	K [kPa.s <sup>-n</sup> ]	$g_s$ [-]	$Y_0^T$ [kPa]	$q^T$ [kPa]	$b^T$ [-]	$h^T$ [kPa]	$Y_0^C$ [kPa]	$q^C$ [kPa]	$b^C$ [-]	$h^C$ [kPa]
565	1050	.907	583	585	3000	920	0.	<b>5450</b>	24.8	1560
570	500	.7907	4.	75.	159	400	0.	<b>2006</b>	12.3	20



### 3.2 Shear tests on A356 suspensions

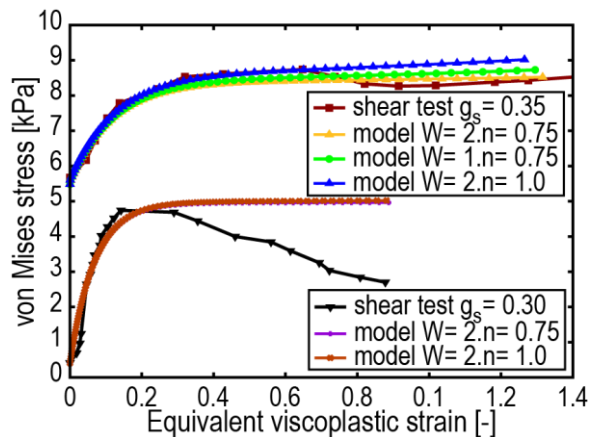


**Figure 3:** Model identification of shear jump tests on suspensions ( $g_s = 0.3$  and  $g_s = 0.35$ ).

A Searle rheometer was used to perform shear rate jump experiments on semi-solid suspensions. Results at  $D^{vp} = 0.005 \text{ s}^{-1}$  for  $g_s = 0.35$  and  $0.30$  are displayed in Figure 3. Linear stress increase occurs until yielding happens at few kPa, then stress decreases due breaking of dendrite entanglements. Model predictions have been realized for different combinations of unknown exponents  $w$  and  $n$ . They show clearly that combination  $w = 2$  and  $n = 1$  leads to the most accurate flow curve for both simulated suspensions. Moreover, the fact, that  $n = 1$  is more accurate, underlies that both identified A356 suspensions behave like a Newton fluid.

## 4. Conclusions

Specific viscoplastic constitutive laws have been derived for the coherent and non-coherent regimes of a semi-solid alloy during solidification and remelting. Continuity between the laws has been expressed at traction and shear coherency and at  $T_{liq}$  and  $T_{sol}$ , such that a continuous transition is guaranteed from pure viscous melt flow to an elastoplastic behaviour at room temperature. The model parameters have been identified successfully for isothermal uniaxial tension, compression and shear tests of an A356 aluminium alloy. In near future, this model will be used in casting simulations and extended to handle also kinematic hardening (e.g. backstress) and decohesion in tension. However, the real challenge will be to identify for each material parameter of the presented constitutive laws, the relevant microstructural features by adoption a multiscale simulation strategy for casting and welding processes.

## Acknowledgments

The authors acknowledge the financial support from the DFG in the framework of the collaborative research centre SFB 1120 “Precision Melting Engineering” and B. Zhou and M. Budnitzki (TU Bergakademie Freiberg) for the interesting discussions.

## References

- [1] Martin C L, Favier D and Suéry M 1997 *Int. J of Plasticity* **13** 215-235.-
- [2] Martin C L, Braccini M and Suéry M 2002 *Mater. Scien. & Engng. A* **325** 292-301.
- [3] Ludwig O, Drezet J-M, Martin C and Suéry M 2005 *Metall. & Mater. Trans. A* **36** 1525-35.
- [4] Mihanyar S, Mo A, M’Hamdi M, Ellingsten K 2011 *Metall. & Mater. Trans. A* **42** 1887-95.
- [5] Zavaliangos L and Anand L 1993 *J. Mech. & Phys. Of Solids* **41** 1087-1118.
- [6] Laschet G, Vossel T, Wolff N, Apel M and Bührig-Polaczek A 11 2017 *Proc. 6<sup>th</sup> Int. Conf. on Solidification Processing (SP17)* 576-580
- [7] Dziallach S, Benke S, Prah U and Bleck W 2009 *Int. J of Cast Metals Res.* **22** 248-51.
- [8] Benke S, Dziallach S, Laschet G, Prah U and Bleck W 2009 *Comput. Mat. Sci.* **45** 633-37.
- [9] Chiumenti M, Cervera M, Dialani N, Wu B and Jinwei J 2016 *FE in Anal. & Des.* **121** 118-133.
- [10] Benke S, Laschet G 2008 *Solid State Phenomena* **141-143** 653-658.
- [11] Moll A, Modigell M., Caylak I, Mahnken R 2010, final report of DFG project about “experimental characterization and modelling of suspension in casting processes”
- [12] Lemaitre J, Chaboche J.-L. 1990 *Mechanics of Solid Materials* (Cambridge, Cambridge University Press).
- [13] Decultieux F, Ph D thesis at ParisTech, 1996.